Molecular Therapy
Original Article

APOE2 gene therapy reduces amyloid deposition and improves markers of neuroinflammation and neurodegeneration in a mouse model of Alzheimer disease

Rosemary J. Jackson,[1,2] Megan S. Keiser,[3] Jonah C. Meltzer,[1,2] Dustin P. Fykstra,[1,2] Steven E. Dierksmeier,[1,2,5] Soroush Hajizadeh,[6,8,9] Johannes Kreuzer,[6,7] Robert Morris,[6] Alexandra Melloni,[1] Tsuneo Nakajima,[1,2] Luis Tecedor,[3] Paul T. Ranum,[3] Ellie Carrell,[3] YongHong Chen,[3] Maryam A. Nishtar,[1,2] David M. Holtzman,[10] Wilhelm Haas,[6,7] Beverly L. Davidson,[3,4] and Bradley T. Hyman[1,2]

[1]Alzheimer Research Unit, Massachusetts General Hospital Institute for Neurodegenerative Disease, Charlestown, MA 02129, USA; [2]Department of Neurology, Massachusetts General Hospital and NeuroDiscovery Center, Harvard Medical School, Boston, MA 02114, USA; [3]Raymond G. Perelman Center for Cellular and Molecular Therapeutics, Children's Hospital of Philadelphia, Philadelphia, PA 19104, USA; [4]Department of Pathology and Laboratory Medicine, Perelman School of Medicine, University of Pennsylvania, Philadelphia, PA 19104, USA; [5]Medical Sciences Division, University of Oxford, Oxford OX3 9DU, UK; [6]Krantz Family Center for Cancer Research, Massachusetts General Hospital, Boston, MA 02114, UK; [7]Department of Medicine, Harvard Medical School, Boston, MA 02115, USA; [8]Broad Institute of MIT and Harvard, Cambridge, MA 02142, USA; [9]Institute of Molecular Biosciences, University of Graz, 8010 Graz, Austria; [10]Department of Neurology, Hope Center for Neurological Disorders, Knight Alzheimer's Disease Research Center, Washington University in St. Louis, St. Louis, MO 63108, USA

Epidemiological studies show that individuals who carry the relatively uncommon APOE ε2 allele rarely develop Alzheimer disease, and if they do, they have a later age of onset, milder clinical course, and less severe neuropathological findings than people without this allele. The contrast is especially stark when compared with the major genetic risk factor for Alzheimer disease, APOE ε4, which has an age of onset several decades earlier, a more aggressive clinical course and more severe neuropathological findings, especially in terms of the amount of amyloid deposition. Here, we demonstrate that brain exposure to APOE ε2 via a gene therapy approach, which bathes the entire cortical mantle in the gene product after transduction of the ependyma, reduces Aβ plaque deposition, neurodegenerative synaptic loss, and, remarkably, reduces microglial activation in an APP/PS1 mouse model despite continued expression of human APOE ε4. This result suggests a promising protective effect of exogenous APOE ε2 and reveals a cell nonautonomous effect of the protein on microglial activation, which we show is similar to plaque-associated microglia in the brain of Alzheimer disease patients who inherit APOE ε2. These data increase the potential that an APOE ε2 therapeutic could be effective in Alzheimer disease, even in individuals born with the risky ε4 allele.

INTRODUCTION

Inheritance of the ε4 allele of apolipoprotein E (APOE) is the strongest genetic risk factor associated with the sporadic form of Alzheimer disease (AD), increasing risk by >10-fold compared to the common APOE ε3/3 genotype. By contrast, the rare APOE ε2 allele has the opposite effect,[1,2] and individuals with APOE ε2/2 rarely develop AD. The presence of even a single allele of APOE ε2 in individuals who are APOE ε2/3 or APOE ε2/4, have improved phenotypes compared to APOE ε3/3 or ε4/4, respectively.[2–6] APOE ε2 carriers who do develop AD have a later age of onset, a slower rate of progression, and fewer neuropathological changes in their brains.[5,7,8] These data suggest one of two possibilities: that APOE ε2/4 and APOE ε2/3 heterozygotes show benefits due to either a beneficial effect of APOE2 itself or a lowered dose of more toxic APOE4 or APOE3; our current experiment was designed to provide data to inform about these possibilities.

APOE isoform has been shown to correlate with several AD-related phenotypes. APOE4 has been shown to increase the aggregation of amyloid-β (Aβ) as well as decrease the clearance of Aβ across the blood-brain barrier (BBB).[9–12] This is associated with increased Aβ deposition in patients with AD, and this strong APOE4- and APOE2-associated phenotype is replicated in targeted replacement animal models in which APOE ε4 carriers have more plaque deposition than APOE ε3 carriers, and APOE ε2 carriers have the lowest plaque deposition of all.[9,13] APOE4 markedly enhances tau-related toxicity in animal models as well.[14] APOE4 is known to be associated with synapse loss near plaques in AD patients.[15,16] Finally, APOE4 has also been shown to affect neuroinflammation. APOE4 in

Received 17 July 2023; accepted 15 March 2024;
https://doi.org/10.1016/j.ymthe.2024.03.024.

Correspondence: Rosemary J. Jackson, Alzheimer Research Unit, Massachusetts General Hospital Institute for Neurodegenerative Disease, Charlestown, MA 02129, USA.
E-mail: rjackson12@mgh.harvard.edu

microglia leads to a robust "proinflammatory" phenotype, although whether this is due to a cell-autonomous or noncell-autonomous mechanism is unknown.[17] Although the exact mechanism of APOE4 action in amyloid deposition, synapse loss, and neuroinflammation is unknown, it appears that in both humans and murine models, inherited APOE2 prevents or delays these features.[7,8]

APOE is a secreted protein predominantly expressed by astrocytes and microglia in the CNS; peripherally it is largely made in the liver. The BBB precludes APOE transport in both directions, so that CNS APOE reflects only protein manufactured within the CNS.[18] Adeno-associated virus (AAV)-derived introduction of APOE2 into mice that develop plaques has been shown, both by our group and others, to prevent plaque formation and even shrink plaques that have already been deposited.[19–21] AD affects the entire cortical mantle, and widespread delivery of AAVs to the brain remains a challenge in humans, which potentially limits the translatability of AAV-mediated therapies. Here, we refined a method to express APOE2 from the ependymal lining of the ventricles, allowing for secretion of APOE2 into the cerebrospinal fluid (CSF), neuropil, and interstitial fluid. Protein produced in these cells is secreted into the adjacent CSF and delivered throughout the brain via ventricular, perivascular, and subarachnoid spaces.[22–24] The method involves the use of an ependymal-specific promoter, von Willebrand factor A domain containing 3A (VWA3A), to restrict expression to ependymal cells, and use of an AAV1-based capsid.[25]

We demonstrate that APOE2 secretion using this method ameliorates the Aβ, neuroinflammatory, and neurodegenerative phenotypes seen in an Aβ-depositing mouse model of AD that has been crossed with human APOE4-targeted replacement alleles to generate an APP/PS1/APOE4/4 model of AD pathology.[26,27] These data allowed us to test the hypothesis that the expression of APOE2 ameliorates the amyloid, neurodegenerative, and neuroinflammatory phenotypes present in this animal model, even in the presence of a full dose of APOE4 from birth. This study tests two alternative models: that APOE2 has a gain-of-function modulatory role in the development and progression of AD pathology or that the benefits of inheriting and APOE2 allele are more likely due to decreasing the amount of the more toxic APOE3 or APOE4. Since our experimental approach was to add APOE2 on top of the natively produced APOE4, the data favor a modulatory effect of APOE2 expression in AD-related pathological changes. Moreover, the effect of the impact of APOE on microglia appears to be not cell autonomous. We further evaluated whether the presence of APOE2 has a similar effect on microglial phenotype in human AD tissue and found that plaque-associated microglia in APOE2 carriers have less-active characteristics. Together, these data suggest that the introduction of APOE2, even without changing APOE4, may be beneficial in patients with the most aggressive common form of late-onset AD.

RESULTS

Intraventricular injection of AAV.APOE2 leads to sustained production of APOE2 in the brain in a dose-dependent manner

Here, we used an AAV1-based capsid that targets broadly throughout the brain and narrowed expression to ependymal cells using a recently described promoter derived from the VWA3A gene.[25] This construct also included an upstream intron to enhance expression, the human APOE2 coding sequence and a bovine growth hormone (bGH) polyadenylation signal (Figure 1A).

We performed a single intracerebroventricular (ICV) injection of this AAV1-based capsid resulting in ependymal expression of APOE2[25] in 4-month-old *Apoe* knockout (KO) mice, which were sacrificed 2 months later (Figure 1B). Injection with $7E^{10}$ viral genomes (vg) of virus into *Apoe* KO mice showed robust expression of APOE2 mRNA in the ependymal cell lining as detected using RNAscope for human APOE (Figure 1C). APOE2 protein was also detected in a tris buffered saline (TBS) extraction of the cortex assessed by western blots and is ∼10% of APOE present in the APOE4 target replacement mice (Figures 1D and 1E).

The AAV.APOE2 was injected ICV at three different doses: low-$7E^{9}$ vg, mid-$2E^{10}$ vg, and high-$7E^{10}$ vg, as well as a vehicle control group into 4-month-old APP/PS1/APOE4 animals. Two months later, DNA extraction from the hindbrain followed by qPCR against the promotor region of the AAV plasmid showed a dose-dependent effect on uptake; three animals showed viral genome copy numbers, similar to that of vehicle and control animals, considered to be background of the qPCR, and were dropped from the study (Figure 1F). Mass spectrometry-based analysis of terminal CSF collection from a subset of mice show that ∼30% of the APOE in the CSF of mid- and high-dose animals is APOE2 and that this is significantly higher than the background seen in vehicle or control mice (Figure 1G). The number of viral genome copies correlates with increased human APOE2 protein (Figure 1H) and shows a V50 (defined as the point half way between the top and bottom of the sigmoidal curve) of $10^{6.1}$, which equates to 1,309,181 vg copies detected (Figure 1I). The ependymal-produced APOE2 protein diffuses throughout the cortex, as shown by its association with plaques throughout the cortical mantle, which can be immunostained with an APOE2-specific antibody (Figure S1).

To understand whether the expression of APOE2 is affecting the expression of APOE4 in these animals, we assessed total APOE levels in the CSF level (Figure S2A) and found them unchanged. The amount of APOE mRNA in the ventricle area is increased by 50% in the high-dose animals (Figure S2B). RNAscope shows that the expression of APOE2 in these animals does not affect the amount of (endogenous) APOE4 mRNA expression in glia near or far from plaques in the cortex (Figures S2C and S2D). These results suggest that the impact of expression of apoE2 protein in the ependyma does not change the amount of APOE4 mRNA in the cortex, consistent with the idea that this gene therapy strategy does not affect APOE4 synthesis.

Expression of APOE2 has a dose-dependent effect on the level of Aβ plaque deposition

At 4 months of age (time of injection) APP/PS1/APOE4 animals show modest plaque deposition, and by 6 months of age (time of necropsy), plaque deposition is well established across the cortex

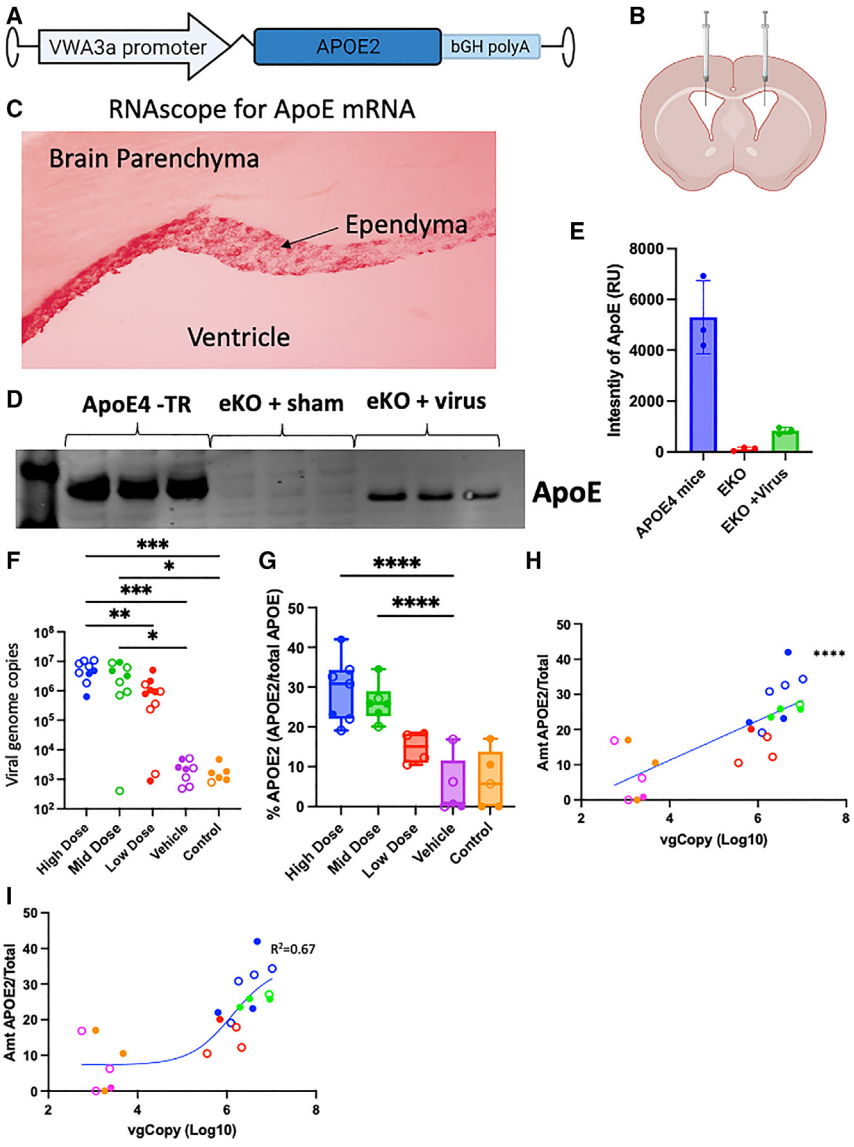

Figure 1. Ependymal cell expression of APOE2 driven by an AAV.APOE1

(A and B) Schematic of the transgene packaged into a modified AAV1 (A) and (B) injected ICV into the mouse brain. (C) *In situ* hybridization showing human APOE expression in the ependymal cells of the ventricle in a *Apoe* KO mouse. (D and E) Western blot (D) for APOE showing that ependymal-expressed APOE2 in the cortex of the *Apoe* KO mice is ∼10% (E) that of the endogenous level. (F) Viral genome copies in tissue extracted from each mouse ($F_{4,35}$ = 5.546, p = 0.0014; post hoc Tukey's multiple comparisons test). (G) Mass spectrometry-determined CSF APOE2 concentration as percentage of total APOE ($F_{4,23}$ = 14.72, p < 0.0001; post hoc Dunnett's test to vehicle). (H and I) The number of viral genome copies detected strongly correlates (H; R^2 = 0.59, p < 0.0001) with the amount of APOE2 detected in CSF (I) and shows a V50 of $10^{6.1}$ when assessed with a Boltzmann sigmoid curve (R^2 = 0.67). n indicated as each mouse is an individual dot. *p < 0.05; **p < 0.01; ***p < 0.001; ****p < 0.0001. Bar graphs show mean ± SD, Box and whisker plots show median, interquartile range and min to max.

(Figure S3). Using ThioS as a marker for dense core amyloid plaques, we show an effect of APOE2 leading to reduced plaque deposition (Figures 2A–2C). The high-dose animals show a significant ∼33% reduction in the percentage of the cortex covered by ThioS$^+$ staining as compared with the vehicle-treated animals (Figure 2B). The dose-dependent effects of APOE2 on plaque burden correlate with the amount of DNA expression seen in each individual animal (Figure 2C). Staining using an anti-Aβ antibody showed a similar trend at both the group (Figures S4A and S4B) and individual levels (Figure S4C).

This reduction corresponds to both a significant reduction in plaque density (Figure 2D) and an even more significant reduction in the size of Aβ plaques (Figure 2E) when high-dose animals are compared with vehicle-treated animals.

Biochemical measures of amyloid align with and confirm the pathological measures. The concentrations of Aβ42 peptides measured from the formic acid and SDS-soluble extracts of mouse brain mimicked the changes observed histologically such that the high-dose animals showed a ∼50% reduction in the amount of both SDS- (Figure S4D) and formic acid (Figure S4E)-soluble Aβ42.

Expression of APOE2 has a dose-dependent effect on plaque-related neuroinflammation

Data from human patients show that microglia in APOE ε4 patients have a more inflammatory phenotype than APOE ε3 or 2 individuals.[17] To determine whether the addition of APOE2 could attenuate the effect of plaques on plaque-associated glia, we performed immunohistochemistry (IHC) for Aβ, Iba1 (microglia) (Figures 3A and S5A), and glial fibrillary acidic protein (GFAP) (astrocytes) (Figures S5A and S5B). We assessed the level of plaque-associated glial reactivity on a semiquantitative 4-point scale where 1 is non-reactive and 4 is very reactive, assessing the areas immediately surrounding the plaque (Figure S5A). The scale was validated by having the images assessed by 2 independent investigators (R.J.J. and B.T.H.), with a correlation R^2 of 0.89.

Microglial reactivity was significantly reduced in the high- and mid-dose mice when compared with the vehicle-treated controls (Figures 3B and 3C), and this attenuation showed a significant dose-response correlation (Figure 3C). This attenuation appears to be driven by an increase in the number of plaques that are not associated with a strong microglial reaction (score of 1) in

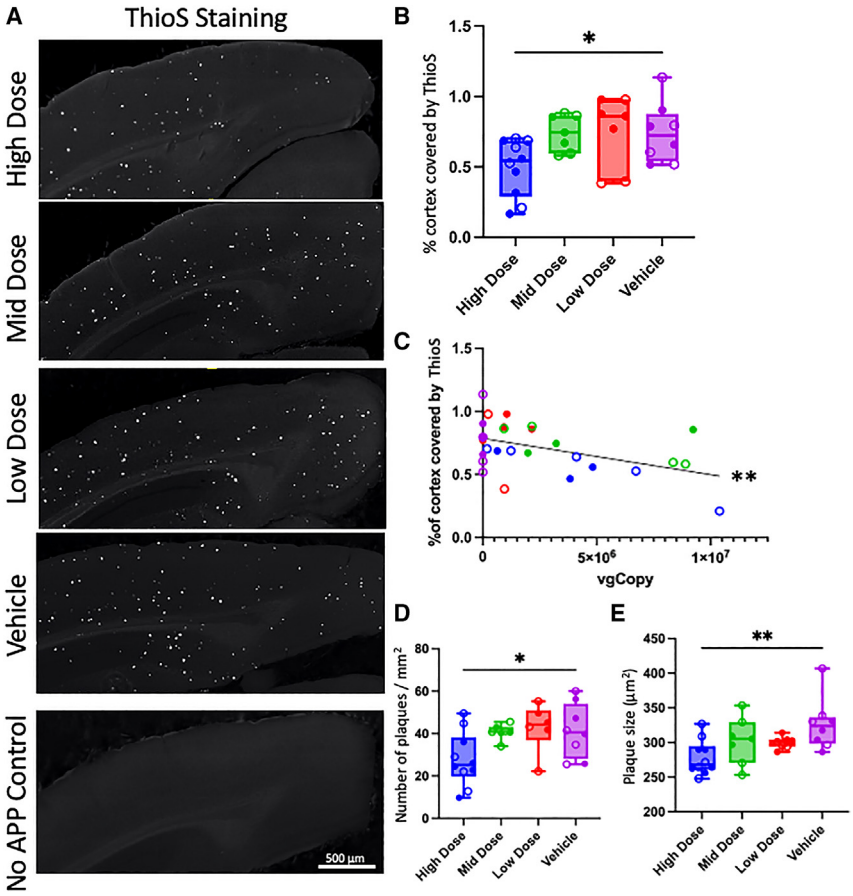

Figure 2. APOE2 reduces plaque deposition, number, and size in a dose-dependent manner

(A) IHC for ThioS in the cortex of dosed APP/PS1/APOE4 animals. (B) Percentage of cortex coverage by ThioS staining is significantly lower in the high-dose animals ($F_{3,27}$ = 4.310, p = 0.0329). (C) The percentage of cortical coverage by ThioS is significantly correlated (p = 0.01) to the number of viral genome copies in the brain sample from each mouse. (D and E) Plaque number (D) ($F_{3,27}$ = 3.597, p = 0.0263) and plaque size (E) ($F_{3,27}$ = 4.113, p = 0.0159); both show a significant effect in the high-dose group. n indicated as each mouse is an individual dot, with open circles as females and closed circles as males. Post hoc tests are shown as Dunnett's multiple comparisons test compared with vehicle. *p < 0.05; **p < 0.01. Box and whisker plots show median, interquartile range and min to max.

the high- and mid-dose animals and a corresponding reduction in plaques that have a score of 4 as compared with vehicle-treated animals in which almost all of the plaques are associated with highly reactive microglia (Figure 3D). We further assessed the local activation state of microglia by using RNAscope probes for the homeostatic microglial marker P2ry12 and the damage-associated microglial marker Clec7a in 3 high-dose and 3 vehicle-treated animals, with microglial response scores nearest the mean and equivalent RNAscope^{+} control probe intensity (Figure 3E).[28] P2ry12 puncta are found in cells that are reasonably evenly spread throughout the cortex, although there are microglial clusters of cells near plaques, whereas Clec7a mRNA is found predominantly in cells in the immediate vicinity of plaques. We assessed 50 plaques and 50 non-plaque regions per mouse, as well as the periplaque area, here defined as the region <25 µm from the edge of the plaque halo, and we saw no change in the amount of P2ry12 puncta per microglia when comparing plaque proximity or treatment group (Figure 3F). These data show a significant difference between treatment groups in the number of Clec7a transcripts in both the periplaque and plaque areas (Figure 3G), confirming the morphological data (Figure 3C) with a molecular marker of disease-associated microglial activation.[29]

Meanwhile, astrocyte reactivity around plaques is unaffected by APOE2 levels or expression (Figures S5C–S5E) and is equally elevated around plaques in all of the groups.

APOE2 exposure improves measures of synaptic loss around amyloid deposits

Synapse loss is known to correlate with cognitive impairment and has been shown to occur near plaques in human patients,[16] as well as in this mouse model,[19] with higher amounts of synaptic loss near plaques in APOE4 compared with APOE3 mice or carriers.

Postsynaptic densities (PSD95) were stained using IHC and imaged using a confocal microscope (Figure 4A). Synapse loss in this model has previously been shown to occur within ~15 µm of the edge of a plaque.[19] We, therefore, measured synapse density within the halo of expected synapse loss (within 15 µm of the plaque edge), as well as in an area far from plaques where synapse density would be expected to be normal (>40 µm from the plaque edge). As expected, synapse density far from plaques did not differ among groups and did not differ from APOE4 mice with no APP/PS1 expression (i.e., control) (Figure 4B). We were excited to find that the high-dose animals showed an increased level of synapses near plaques as compared with vehicle-treated animals (Figure 4C), restoring this marker of neurodegeneration to near-normal levels. Percentage of synapse loss was calculated by comparing the synaptic density near plaques with the synaptic density far from plaques within the same animal (Figure 4D). Vehicle-treated animals show twice as much synapse loss as high-dose animals, with 70% of high-dose animals showing <10% loss near plaques as compared with the other groups where all but 1 mid-dose animal showed >10% loss.

We also evaluated the number of dystrophic neurites associated with amyloid deposits by staining for the axonal marker SMI312 alongside

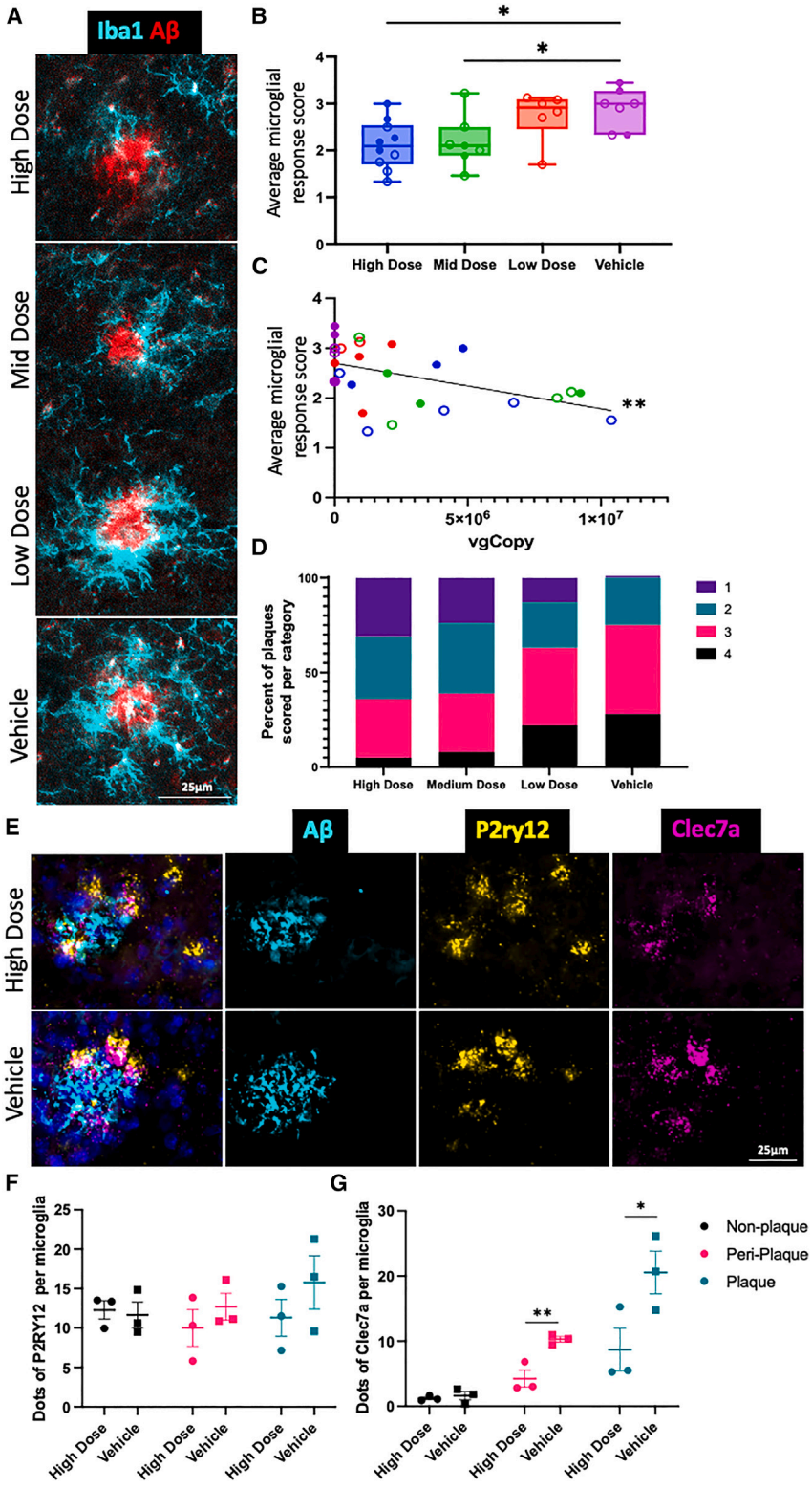

Figure 3. APOE2 reduces microgliosis near plaques

(A) IHC for IBA1 and Aβ in the cortex of dosed APP/PS1/APOE4 animals. (B and C) Average microglial response score (B) ($F_{3,26}$ = 4.529, p = 0.0110) shows a reduction in microglial activation in the high- and mid-dose groups, and (C) is significantly correlated (p = 0.0081) to the number of viral genome copies in that mouse. (D) This reduction is due to a decrease in the number of plaques scored as a 4 and an increase in the number of plaques scored as a 1. n indicated as each mouse is an individual dot, with open circles as females and closed circles as males. Post hoc tests are shown as Dunnett's multiple comparisons test compared with vehicle. (E and F) RNAscope for P2ry12 and Clec7a of high-dose and vehicle-treated animals (E) shows that there is (F) no change in the number of P2ry12 transcripts per microglia. (G) In the treated animals, there is a significant attenuation in the number of Clec7a transcripts per microglia in the plaque area (p = 0.0317) and the periplaque area (p = 0.0057) in the high-dose animals compared with controls. *p < 0.05; **p < 0.01. Box and whisker plots show median, interquartile range and min to max, scatter dot plots show mean ± SEM.

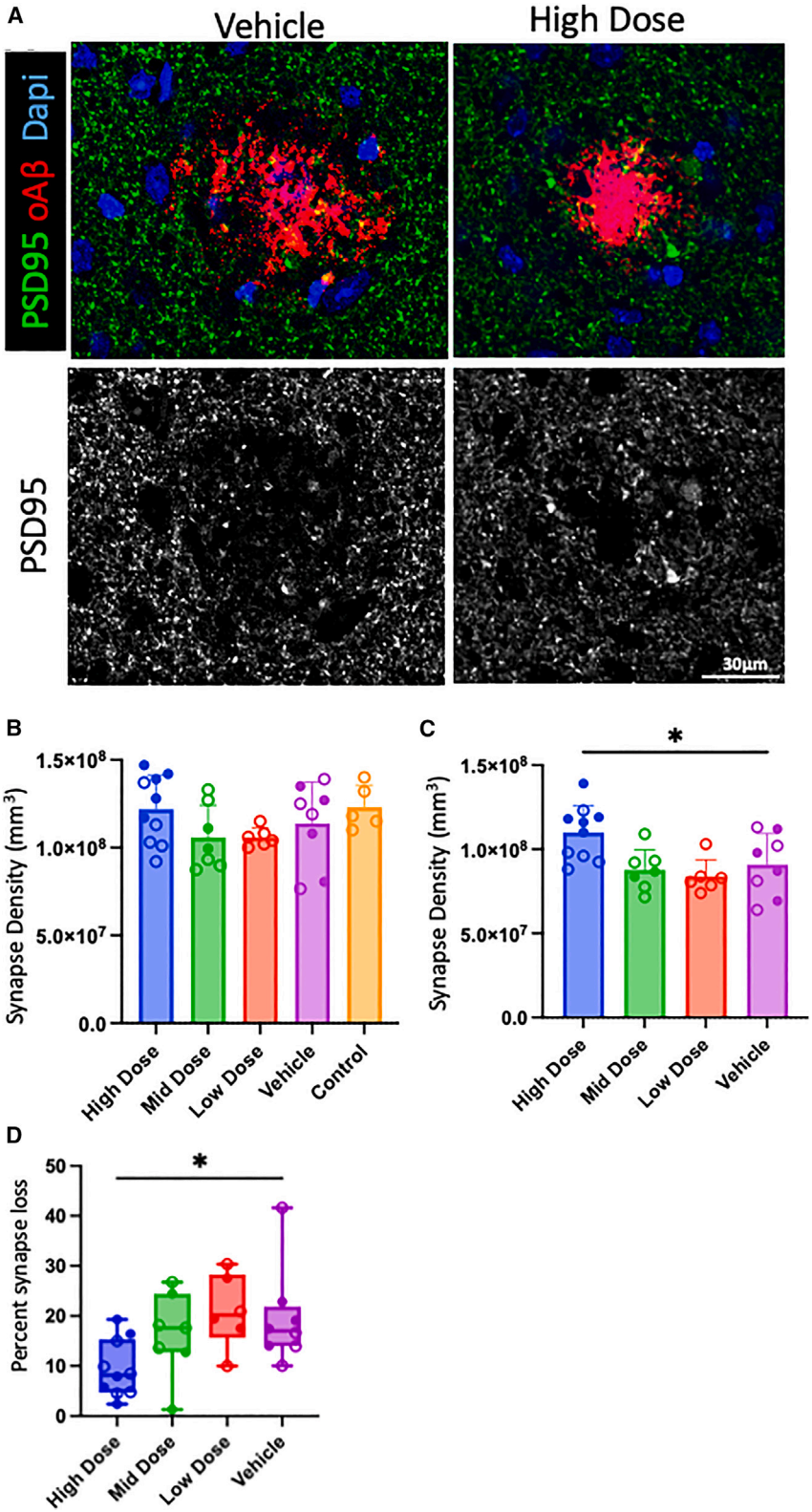

Figure 4. APOE2 reduces synaptic loss near plaques

(A) IHC for PSD95 and Aβ in the cortex of dosed APP/PS1/APOE4 animals. (B and C) Synapse density is unchanged far from plaques (B), but (C) significantly increased near plaques ($F_{3,27}$ = 5.153, p = 0.0060). (D) This leads to a significant decrease in the percentage of synapse loss in the high-dose animals compared with vehicle ($F_{3,27}$ = 3.693, p = 0.0239). n indicated as each mouse is an individual dot, with open circles as females and closed circles as males. Post hoc tests are shown as Dunnett's multiple comparisons test compared with vehicle. *p < 0.05. Bar graphs show mean ± SD, box and whisker plots show median, interquartile range and min to max.

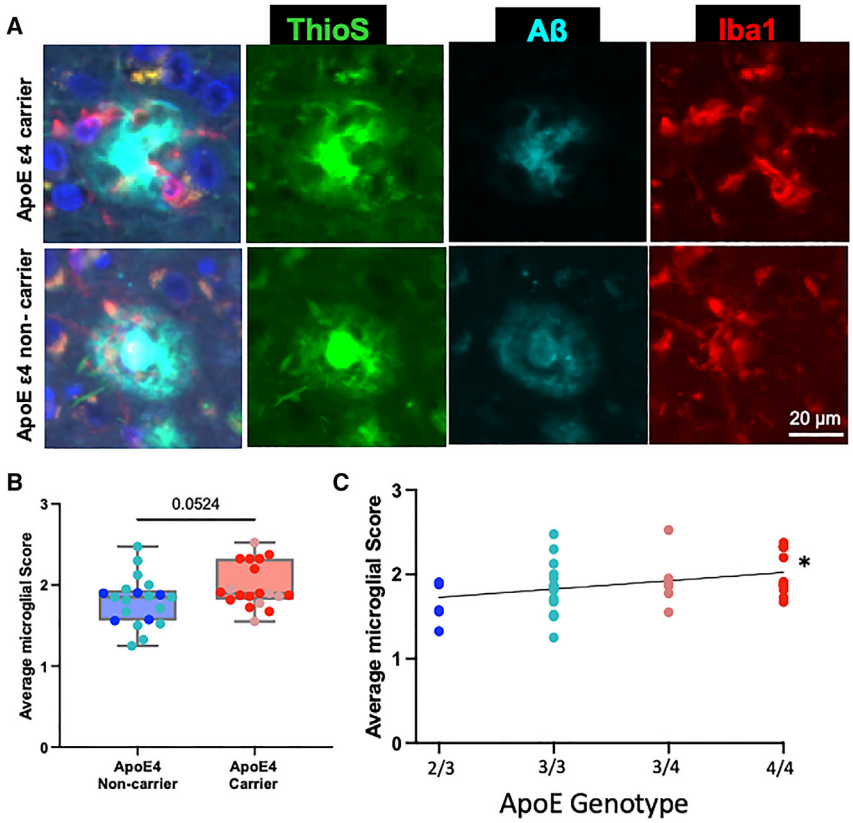

Figure 5. APOE2 reduces microgliosis near plaques

(A) IHC for IBA1 and Aβ in the frontal cortex of postmortem tissue from end-stage human AD cases. (B) Average microglial response score (t_{37} = 2.0, p = 0.0524) shows an increase in microglial activation in APOE4 carriers compared with noncarriers. (C) There is a significant correlation between microglia activation and APOE risk (where APOE2/3 individuals are assessed as having −1 APOE4 allele) ($F_{1,35}$ = 5.410, p = 0.0259). *p < 0.05. Box and whisker plots show median, interquartile range and min to max.

an Aβ antibody (Figure S6A). In this model, these dystrophic neurites generally do not immunostain for abnormal tau epitopes, and there is not a strong tau phenotype. We found no difference in the number of axonal neuritic dystrophies among the groups (Figures S6B and S6C).

APOE isoform has an effect on plaque-related neuroinflammation in humans

To assess the translatability of our findings, we looked at microglia in the immediate vicinity of plaques in frontal cortex collected from individuals with a neuropathological diagnosis of AD and known ApoE genotypes (Figure 5A; Table S1). We again assessed the level of plaque-associated microglial reactivity on a semiquantitative 4-point scale, where 1 is nonreactive and 4 is very reactive, assessing the areas immediately surrounding the plaque. Overall plaques in human tissue show a lower level of microglial reactivity than those in mice (Figures 3B and 5B), potentially due to the speed of plaque formation or the amount of soluble Aβ produced in mice with familial AD mutations. There was a significant correlation of microglial reactivity with the number of APOE alleles (where APOE2/3 individuals were considered to have −1 APOE4 alleles) (Figure 5C). This translated into a trend toward an increased level of microglial reactivity in APOE4 carriers compared with noncarriers (Figure 5B).

DISCUSSION

The strong genetic and experimental link between APOE genotype and AD has long made APOE a subject of interest when considering AD risk modifiers or therapeutics.[5,7] Although APOE4 is unequivocally associated with a more aggressive AD phenotype, the protective effect of APOE2 has been attributed to it acting as a null, reducing the dose of the more toxic forms of APOE. In contrast, we hypothesized that APOE ε2 may have a positive modulatory impact on neurodegenerative processes, leading to a beneficial gain-of-function mechanism, or at least to a function that blocks potentially toxic effects of the risk alleles. For example, APOE2 protein has far less binding to the low-density lipoprotein (LDL) receptor than other isoforms, although this is not true of binding to other members of the LDL receptor family.[30] Our data suggest strongly that the latter is the case, since expression of a relatively small amount (∼30% of basal amounts) of APOE2, in the setting of continued unchanged amounts of APOE4, strongly affect AD-related phenotypes. The relatively small amount of APOE2 present suggests that the effect is a therapeutic beneficial gain of function, rather than (only) a diminished amount of APOE4 synthesis. Importantly, in either case, this improvement is observed in the setting of mild but already-established plaque deposition and continued APOE4 expression, showing that the effect of APOE2 actively modulates the impact of APOE4.

The practical issues of distributing gene product throughout the brain is a barrier to using gene therapy in widely distributed diseases such as AD. This is especially true in larger organisms such as nonhuman primates or humans in whom the diffusion rate of injected material through the brain parenchyma limits the ability of a single AAV injection to affect large areas of brain. Our current and previous studies suggest an approach to overcome this barrier: expression of secreted proteins via transduction of the ependyma and related structures, allowing secreted protein to diffuse throughout the cortical mantle.[19,24,31] The diffusion rate of AAV through the CSF held in the ventricle is much greater than that of the relatively solid parenchyma, and the ependymal cell layer of the ventricle is important for the maintenance and production of the CSF.[32] Thus, transfection

of these cells allows for gene product to be pumped out into the CSF, where it can affect the entire cortical mantel and makes for an attractive method of overcoming the limitations introduced by a larger target area in the jump from rodent models to humans.

We applied this approach to expressing APOE2 in an APP/PS1/APOE4 model of AD pathology, and shows that in achievable doses, expression of APOE2 secretion into the neuropil can positively affect plaque deposition, neuroinflammation, and neurodegeneration within a short time interval—8 weeks. The effect of APOE2 on plaques is expected from a robust neuropathological literature showing that APOE ε2 carriers have fewer plaques. The results here suggest that the impact of APOE in AD is ongoing, and that manipulating APOE even after plaques are established can alter the course of the disease. Previous work from the group has shown that APOE2 gene therapy is able to not only slow but also slightly reverse already-established plaque deposition, and we postulated that this could be due to effects on Aβ clearance.[19] In particular, APOE2 has been shown to increase the clearance of Aβ across the BBB and well as decrease aggregation, because previous studies have shown APOE effects for both the clearance and aggregation of Aβ.[7,9,12] The positive APOE2 effect we see is on both dense core fibrillar plaques and biochemical measures of Aβ, consistent with the interpretation that APOE2 is actively facilitating increased clearance of Aβ across the BBB.

Neuroinflammation and AD have been linked in part due to the number of microglial genes that are risk factors for AD[33] and the marked increase in micro- and astrogliosis in brains from both AD cases and mouse models.[34,35] Microglia produce APOE under basal conditions, but production is dramatically increased in these cells in the context of AD, leading to the hypothesis that microglial-produced APOE4 has a toxic cell autonomous gain-of-function effect.[29] By contrast with this expectation, our current data show that exogenous APOE2 has a dampening effect on microglial activation near plaques in these mice (Figure 3), consistent with an additional noncell-autonomous effect. The effect of APOE2 on microglia in this paper is reminiscent of the depressed microglial response seen in TREM2 KO mice,[36] but here, we do not see a concurrent increase in neuritic dystrophies or synaptic loss that is seen in those models.[37]

Importantly, this effect of APOE on microglial reactivity to plaques is also seen in human AD cases despite the heterogeneity and relatively end-stage nature inherent in studying human brain tissue (Figure 5). Here, we showed a modest increase in microglial reactivity score when comparing APOE4 carriers to noncarriers. This increase occurs stepwise with relative APOE risk because a test for linear trend is significant (Figure 5).

APOE4 has been associated with more severe synapse loss near plaques in AD in both human and mouse models.[16,19] In this mouse model of AD, we see a loss of synapses near plaques; however, this synapse loss is lessened in the mice expressing APOE2. This could be due to reduced levels of synaptic pruning due to less active microglia or to reduced bioactive oligomeric Aβ (oAβ). Alternatively, or in addition, we have previously shown that APOE and oAβ colocalize at the synapse,[16,38] and we postulated that the interaction of oAβ with APOE2 rather than APOE4 could ameliorate synaptotoxic effects. Whether the interaction of APOE2 with oAβ, or the reduction in synaptotoxic phenotype of activated microglia, or both improve the synapse loss around plaques, the observation that APOE2 expression can improve a core feature of neurodegeneration suggests a potential role for this approach in a therapeutic context. This reduction in plaque-associated microgliosis and synapse loss also indicates that despite the presence of plaques, APOE2 can prevent those features of AD that are more tightly linked with cognitive decline (e.g., synapse loss),[39] ameliorating the impact of already-established plaques while reducing the deposition of new plaques.

Aβ immunotherapy[40,41] leads to profound plaque reduction and modest cognitive gains and has been recognized by US Food and Drug Administration approvals. In contrast to Aβ immunotherapy, APOE2, while also affecting plaques, does not rely on the activation of microglia and increased neuroinflammation to modulate plaques, and appears to dramatically quench existing inflammatory microglial signatures and restore synaptic integrity. Indeed, an early-phase clinical trial using APOE2 gene therapy has shown some promise in a small number of participants[20] (Clinicaltrials.gov: NCT03634007). That method uses a modified AAV10 and showed promise in animal models before being translated to humans.[21] We posit that by restricting expression to the ependymal cells, we can minimize potential off-target effects, prevent possibly deleterious neuronal APOE expression, and provide support for an alternative delivery strategy of this gene therapy approach.[25] Taken together, these results suggest that APOE2 is a promising approach for potential therapeutic development in AD and related disorders and that this method of gene therapy delivery could benefit patients with APOE ε4 driver of their disease.

MATERIALS AND METHODS

Study design

Mice were randomly assigned to treatment groups and injected with AAV.APOE2 or a vehicle control 4 months after birth. The impact of human APOE2 on amyloid deposition was assessed 2 months later by IHC and ELISA. Study groups were blinded to the investigator. We calculated that 8 animals (4 of each sex) per condition would provide a power of >0.8 for a 30% correction of baseline phenotypes based on prior data.[19]

Animals

APP/PS1[27] mice express human mutant APP KM670/671NL and PSEN1 L166P under the Thy1 promotor and have amyloid deposition at 3–4 months of age. This strain was then crossed with humanized APOE4 mouse wherein the mouse *apoE* was replaced with human APOE4.[26] Four-month-old APOE4-TR/APP/PS1 mice were dosed with high (7E−10 vg, n = 11), medium (2E−10 vg, n = 9), or low (7E−9 vg, n = 12) AAV.APOE2 or a vehicle control (n = 9) and studied for 2 months. A cohort of APOE4 littermates (n = 12) lacking APP/PS1 transgenes were scarified at 6 months to use as a control

for APP expression. A cohort of *Apoe* KO (The Jackson Laboratory) mice on a C57BL/6 background was included to assess Aβ background levels in tissue and CSF. Experiments were performed in accordance with the NIH and institutional guidelines and both sexes were used. Due to the small size of the mouse brain, not all of the animals were used in every analysis. Table S2 indicates which animals were included in each analysis. Open circles indicate females and closed circles indicate males. All animal care, housing and experiments were performed in compliance with the guidelines established by the Massachusetts General Hospital institutional animal care and use committee and in accordance with the National Institutes of Health Guide for the Care and Use of Laboratory Animals.

Viral vector construction and production

The proviral APOE2 construct was generated as described previously.[25] Briefly, a genomic region upstream the human VWA3a gene (GRCh38/hg38, chr16:22090639-22092605) was PCR amplified (forward 5′-TCCTGGATGGGACCACGCTAG-3′; reverse 5′-GCACTCCAG GGCCTTACTTCTC-3′) to serve as an ependyma-enriched promoter. A chimeric intron derived from human β-globin and immunoglobulin heavy-chain genes was appended immediately downstream to enhance expression. The human APOE2 coding sequence (Acc. NP_000032.1 containing an R176C mutation) initiated by a strong Kozak sequence (GCCACCATG), was placed downstream and terminated with a bGH polyadenylation signal. The entire transgene was flanked by AAV2 inverted terminal repeats. Transgenes were packaged using standard triple transfection procedures into an AAV1-based capsid that targets broadly throughout the brain, including in the ependyma. AAVs were manufactured by the Children's Hospital of Philadelphia Research Vector Core and resuspended in diluent buffer (Research Vector Core). Quality testing and titering were performed in-house by the Research Vector Core. Quality control and test methods, with procedures and results, were reported on a certificate of analysis for each lot.

Stereotactic ICV injections

AAV ICV injections were performed as described previously.[14,30] Animals were anesthetized (O_2/isoflurane 0.2%) and positioned on a stereotactic frame (David Kopf Instruments). Injections were performed in each lateral ventricle with 5.25 μL of viral preparation using a 33G needle attached to a 10-μL Hamilton syringe (Hamilton Medical) at 0.20 μL/min. Stereotactic coordinates were calculated from bregma (anteroposterior +0.3 mm, mediolateral ±1 mm, and dorsoventral −2 mm).

Mouse processing

Mice were euthanized by isoflurane inhalation. One cerebral hemisphere was fixed in 4% paraformaldehyde and 15% glycerol in PBS and switched to 30% glycerol in PBS 48 h later. The remaining hemisphere was subdivided and snap-frozen for biochemical analysis. Drop fixed hemispheres were processed by neuroscience associates. A total of 40 hemispheres were embedded in a gelatin block and sectioned to 30 μm.

Western blot

Mouse cortical tissue was homogenized in 10 vol by weight of ice-cold Tris-buffered saline (TBS) with protease and phosphatase inhibitors using a handheld electric homogenizer. The homogenate was then spun at 10,000 × *g* for 10 min and the supernatant (TBS-soluble fraction) was collected for western blot. Protein concentration was determined using a bicinchoninic acid assay. Total protein (5–10 μg) was loaded and separated by 4%–12% NuPAGE gels in 2-(*N*-morpholino)ethanesulfonic acid buffer, and proteins were then separated by weight for 2 h at 120 V. Proteins were electrotransferred onto nitrocellulose membrane at 30 V for 1.5 h using the XCell II Blot Module system in Tris-glycine transfer buffer. Membranes were incubated in blocking buffer (Li-Cor Biosciences) diluted 1:1 TBS for 1 h to reduce background staining. Membranes were then incubated with primary antibodies; rb anti-APOE (Novus Biologicals, NBP1-31123), and ms anti-glyceraldehyde 3-phosphate dehydrogenase (Millipore, MAB374) diluted in blocking buffer with added 0.1% Tween 20 overnight at room temperature while shaking. Membranes were then washed and incubated with the appropriate 680 and 800 infrared dye secondary antibodies (Li-Cor Biosciences). The membranes were imaged using the Odyssey infrared imaging system and analyzed using Odyssey software.

DNA and RNA extraction and analysis

Genomic DNA was extracted from brain tissue using QIAamp DNA Mini Kit (Qiagen) as per the manufacturer's protocol. Samples were run on Bio-Rad CFX384 Real-Time System C1000 Touch using Bio-Rad CFX Manager 3.1 software. Total genome copies were quantified against a six-point standard curve generated using linearized plasmid containing the construct. Primer/probes (designed against a noncoding region in the construct) was used with TaqMan Master Mix (Applied Biosystems).

Total RNA was extracted from brain tissue using TRIzol (Ambion, Life Technologies) as per the manufacturer's protocol. RNA (1 μg) was treated with DNase I, RNase-free (Thermo Scientific) as per the manufacturer's protocol. cDNA was generated using the High-Capacity cDNA Reverse Transcription Kit (Life Technologies). Samples were run on Bio-Rad CFX384 Real-Time System C1000 Touch using Bio-Rad CFX Manager 3.1 software. APOE levels were quantified by designed primer/probes to be used with TaqMan Master Mix (Applied Biosystems). mRNA levels of human APOE (Hs00171168_m1) were detected using the commercial TaqMan primer/probe set (Applied Biosystems). Endogenous mouse β-actin (Mm02619580_g1) was used as a reference gene to normalize expression across samples.

The ΔΔCt relative quantification method was used to calculate gene expression. Mouse β-actin was used as a housekeeping gene included in the RT^2-Profiler array to normalize for RNA amount. Briefly, the geometric mean of the Ct values of these reference genes was calculated for each mouse and subtracted from the Ct value of each target gene, yielding ΔCt values. For each gene, the average ΔCt value in vehicle-treated mice was then subtracted from the ΔCt value of each sample to obtain the ΔΔCt values. The relative quantification value was calculated as $2^{-\Delta\Delta C}$.

Mass spectrometry

Relative concentrations of APOE2, APOE4, and total APOE were determined by mass spectrometry in a multiplexed manner using tandem mass tag (TMT) barcoding reagents (TMTpro)[42] targeting three peptides: CLAVYQAGAR (APOE2), LAVYQAGAR (APOE4), and LQAEAFQAR (common to APOE2 and APOE4). All of the CSF samples were reduced, alkylated, and immobilized in a 1:1 mixture of hydrophilic and hydrophobic Sera-Mag SpeedBeads (GE Life Sciences) and underwent tryptic digest as previously described.[43,44] A total of 5 μg of the resulting peptides were subsequently labeled using TMTpro reagents as described previously.[43] Final adjustments of the sample amounts in the individual TMT sets were made to obtain the same intensity for the common peptide (LQAEAFQAR) in all of the samples (see below). Data were acquired on an Orbitrap Eclipse mass spectrometer (Thermo Fisher Scientific) equipped with an EASY-nLC 1200 HPLC (high-performance liquid chromatography) and autosampler (Thermo Fisher Scientific), an FAIMS Pro Interface (Thermo Fisher Scientific), and an in-house prepared microcapillary column (inner diameter, 150 μm; outer diameter, 360 μm) packed to a final length of 30 cm with GP-C_{18} beads (1.8 μm, 120 Å, Sepax Technologies). Data were acquired with an in-house-developed method applied via an API provided by Thermo Fisher Scientific. The method was set up to acquire high-resolution (15,000) Orbitrap CID fragmentation MS2 spectra followed by MS3 spectra from the three most intense target peptide fragment ions. MS2 spectra were assigned in real time using an in-house-developed algorithm, and assignments were confirmed postacquisition using a target-decoy database-based assignment validation (false discovery rate [FDR] $\leq$1%). MS3 spectra were acquired in the Orbitrap at a resolution of 50,000. TMT reporter ion intensities were extracted as that of the most intense ion within a 0.03-Th window around the predicted reporter ion intensities in the collected MS3 spectra. In all of the TMT sets of samples, the first four TMT barcoding channels (126, 127n, 127c, and 128n) were used for CSF samples only containing APOE2 (126 and 127n) or only containing APOE4 (127c and 128n), and the other channels were used for replicates of the measured mouse CSF samples. Of all of the MS3 spectra generated in one run, a maximum of three MS3 spectra were selected for further analysis. For the peptides CLAVYQAGAR (APOE2) and LAVYQAGAR (APOE4), MS3 spectra were selected based the maximum difference of signal between the channels containing only the isoform and the channels not containing the isoform. For the common peptide (LQAEAFQAR), the three MS3 spectra which TMT reporter ion intensity showed the highest Pearson correlation among all possible combination of three MS3 spectra were selected for further analysis. TMT reporter ions were summed for the MS3 spectra selected for each peptide, and for the APOE2 and APOE4 MS3 spectra, the average signals detected in the channels not containing the isoform (127c and 128n for APOE2, 126 and 127n for APOE4) were subtracted as noise levels from all of the channels. APOE2 and APOE4 TMT reporter ions were then normalized based on the common peptide TMT intensities detected in the channels only containing APOE2 or APOE4. After this normalization step, relative APOE2 concentrations (percentage of total) were calculated based on the APOE2 and APOE4 TMT reporter ion intensities in the channels of the analyzed samples. Perpendicular distances to the expected x=y line were calculated for all of the samples, and a Grubbs test (Benjamini-Hochberg FDR 0.25) was applied to remove outliers. A Grubbs test (p = 0.05, one round) was also applied to remove APOE2 concentration outliers for each sample group (high dose, mid-dose, low dose, vehicle, and control). As a final step, the median relative APOE2 concentration of vehicle and control samples (not containing any APOE2) was subtracted from all of the averaged APOE2 concentration values. The total APOE concentration was determined by first adjusting common peptide TMT signals based on the sample amount adjustment applied to obtain the same common peptide signal across all of the samples. TMT reporter ion signals across TMT sets were then normalized using the APOE2only and APOE4only channels.

ELISA

The concentrations of Aβ40 and Aβ42 were determined by BNT-77/BA-27 (for Aβ40) and BNT-77/BC-05 (for Aβ42) sandwich ELISA (Wako) according to the manufacturer's instructions. Aβ40 and Aβ42 concentrations were measured in TBS, SDS-soluble, and SDS-insoluble fractions for each mouse. Sections of mouse brain were homogenized in 10 vol (w/v) of TBS buffer with cOmplete Protease Inhibitor Cocktail (Roche), and centrifuged at 100,000 × *g* for 30 min at 4°C. The supernatant was collected and set aside as the TBS-soluble fraction. The pellet was then homogenized in 10 vol (w/v) of TBS buffer containing 2% SDS, incubated at 37°C for 30 min, and then centrifuged at 100,000 × *g* for 30 min at 20°C. The SDS-insoluble pellet was dissolved in 500 μL of 70% formic acid and sonicated on ice at 10% power in 1-min and 30-s intervals until completely dissolved, and then centrifuged at 100,000 × *g* for 30 min at 4°C. The formic acid-soluble supernatant was desiccated by Speed-Vac and then resuspended in 1 vol (w/v) of DMSO. The DMSO-soluble fraction was used as an SDS-insoluble fraction (procedure adapted from Hashimoto et al.. 2020).[45]

RNAscope

The drop fixed hemisphere of the *Apoe* KO mice was sectioned to 30 μm on a freezing ultramicrotome. Three mice per experimental condition (vehicle injection vs. AAV injected) were stained for *APOE* mRNA by RNAscope. RNAscope experiments were performed using the RNAscope 2.5 HD Assay-RED (Advanced Cell Diagnostics) following the manufacturer's recommendations, with minor adjustments. Briefly, for each mouse several sections were baked onto a Superfrost slide for use in *APOE* mRNA quantification. Following target retrieval and protease digestion, probe hybridization was carried out at 40°C for 2 h with hs-APOE (433091), 3-plex Positive Control Probe_Mm (320881), or Negative Control Probe-DapB (310043). After amplification steps to obtain the RNAscope signals, the signal was developed using the included Fast Red. Sections were mounted using Immunomount and imaged using an upright BX51 Olympus microscope at a magnification of 10×.

To assess microglial reactivity to plaque sections from treated and untreated APOE4/APP/PS1 animals, mice were basked onto a

Superfrost slide. Following target retrieval and protease digestion, probe hybridization was carried out at 40°C for 2 h with ms-Clec7a-C1 (532061) and ms-P2ry12-C2 (317601-C2), 3-plex Positive Control Probe_Mm (320881), and Negative Control Probe-DapB (310043). After amplification steps to obtain the RNAscope signals, the signal was developed using TSA-cy3 (Fisher Scientific, NEL744001KT) for C1 probes and TSA-cy5 (Fisher Scientific, NEL745001KT) for C2 probes. Sections were then blocked in 5% normal donkey serum (NDS) in TBS for 1 h before being incubated with 1:1,000 6E−10 (BioLegend, 803004) overnight at 4°C. Sections were then washed and incubated with Donkey anti-Mouse 488 (Invitrogen, A-21202) at 1:500 for 1 h at room temperature. Sections were washed and then counterstained with 1:1,000 DAPI, and mounted using Immunomount and scanned using a NanoZoomer (Hamamatsu) at a magnification of 40×.

To assess APOE mRNA levels in the APOE4/APP/PS1-treated and untreated animals, we used the above protocol with ms-APOE-C1 (REF), which was then amplified using TSA-cy3 (Fisher Scientific, NEL744001KT). A second section was run in parallel using 3-plex Positive Control Probe_Mm (320881) and was treated identically. Sections were then processed for IHC with 6E−10, as stated above.

Qupath was used to assess the number of RNAscope puncta per cell. An experimenter blind to condition annotated 50 plaque and 50 non-plaque regions per mouse (while only the plaque channel was visible). The plaque annotations were then expanded by 25 μm to create the periplaque annotation. All of the annotations were selected for an individual mouse and the positive cell detection tool was used with DAPI for the cell nucleus and maximum nuclear cyanine5 signal to select microglia without biasing for cells with more or less P2ry12. For APOE quantification, the cell detection tool was used with no selection for microglia. The subcellular detection tool was then used for both $P2ry12^+$ and $Clec7a^+$ puncta, APOE puncta, or positive control puncta, with split by shape and intensity selected, and with an expected spot size of 0.5 μm^2, a minimum spot size of 0.25 μm^2, and a maximum spot size of 3 μm^2.

Murine IHC

Sections were permeabilized in 0.5% Triton X-100 for 15 min before being blocked in 0.1% Triton X-100 and 5% normal goat serum for 1 h at room temperature. Incubation with primary antibodies was done overnight at 4°C in 0.05% Triton X-100 and 2.5% normal goat serum. Sections were then washed in TBS, and appropriate secondary antibodies were diluted 1:500 in 0.05% Triton X-100 and 2.5% normal goat serum in TBS at room temperature. Sections were incubated with 1:1,000 DAPI in TBS for 10 min at room temperature, washed, and mounted using Immunomount.

Plaque quantification

Every 10th section was stained as described above using rabbit anti-Abeta (1:500, IBL, 18584) for amyloid beta. Amyloid dense core plaques were labeled by 0.05% ThioS (Sigma-Aldrich) in 50% ethanol before mounting. Sections were mounted and scanned using a NanoZoomer microscope at 40×. Sections were quantified using qupath.[46] For each section, cortical areas were selected, and plaques were identified using an object classifier. The plaque coverage area was assessed as a percentage of the cortical area measured. For plaque size and number, the same size area was selected in the cortex of each animal and plaques were identified using an object classifier.

Glial assessment

Several sections were stained as described above. Primary antibodies were 1:1,000 biotinylated Ms anti-Abeta 82E1 (IBL, 10326), 1:500 GFAP 488 (Millipore, MAB 3402X), and 1:500 rabbit anti-IBA1 (wako 019–19741). Secondaries were Streptavidin Alexa Fluor 568 (Invitrogen, S11226) and Donkey Anti-rabbit 647 (A-31573). Five cortical plaque-containing areas were imaged at random from the somatosensory cortex using an Olympus FV3000 confocal laser scanning microscope at 40×. z stacks were generated, and each plaque was assessed on a four-point scale (Figure S2A) for the level of glial reactivity by two blinded investigators. All of the plaques for an individual mouse were averaged together to generate the graphs in Figures 3B, 3C, S2C, and S2D, and all of the plaques from a given experimental group were assessed for Figures 3D and S4E.

Synapse quantification

Several sections were stained as described above. Primary antibodies were 1:500 rabbit anti-Abeta 1:500 (IBL, 18584) and 1:500 goat anti-PSD95 (Abcam, ab12093). Secondaries were Donkey Anti-goat 488 (Invitrogen, A-11078) and Donkey Anti-rabbit 594 (Invitrogen, A-21207). Five cortical plaque-containing areas were imaged at random from the somatosensory cortex using an Olympus FV3000 confocal laser scanning microscope at 60× using an oil dipping objective. A total of 5 μm of z stack was imaged at a slice size of 0.56 μm. Images were processed using custom ImageJ and MATLAB macros similar to those of Jackson et al.[38] In brief, 10 × 10 μm crops were taken from areas within 15 μm of the plaque halo or >40 μm from the plaque halo. Cellular debris and DAPI were avoided. Crops were thresholded using custom ImageJ macros and synapses were quantified using custom MATLAB macros. All of the crops were averaged together to find a density near and far from plaques for each mouse.

Neurite quantification

Several sections were stained as described above. Primary antibodies were using 1:500 rabbit anti-Abeta 1:500 (IBL, 18584) and 1:500 mouse anti SMI312 (BioLegend, 837904). Secondaries were Donkey Anti-rabbit 488 (Invitrogen, A-21206) and Donkey anti-mouse 594 (Invitrogen, A-21203). Five cortical plaque-containing areas were imaged at random from the somatosensory cortex using an Olympus FV3000 confocal laser scanning microscope at 60× using an oil dipping objective. A total of 20 μm of z stack was imaged at a slice size of 1 μm. Images were quantified using ImageJ by a blinded experimenter who counted the number of dystrophies per plaque and also quantified the plaque area. In images in which more than one plaque was present, the largest plaque was quantified.

APOE2 staining

Several sections were stained as above with notable changes. The primary antibody was 1:200 rabbit anti-APOE2 (Cell Signaling, E7Y30). Primary antibody was incubated at 4°C in 0.05% Triton X-100 and 2.5% normal goat serum for 1 week to ensure maximum penetration of the tissue. Signal was boosted using a Tyramide SuperBoost kit (Invitrogen, B40925) with anti-rabbit 594. Sections were imaged using an Olympus FV3000 confocal laser scanning microscope at 40× and z stacks were generated.

Human IHC

Human participants with AD were selected from the Massachusetts Alzheimer's Disease Research Center brain bank. Human brain tissues were collected with informed consent of patients or their relatives and approval of local insitutional review boards at Massachusetts General Hospital. Paraffin sections, 4 μm thick, were cut onto a Superfrost slide using a microtome. Following deparaffinization and rehydration, sections were boiled in citrate buffer for 20 min before being allowed to cool to room temperature in the citrate buffer. Sections were then washed with TBS and blocked in 10% NDS in TBS for 1 h at room temperature before being incubated with primary antibody overnight at 4°C. Primary antibodies were 1:500 Iba1 (Wako, 019-19741) and 1:1,000 6E−10 (BioLegend, 803004) diluted in 5% NDS in TBS. Sections were then washed and incubated with 1:500 Donkey Anti-rabbit 594 (Invitrogen, A-21207) and 1:500 Donkey Anti-mouse 647 (Invitrogen, A-31571) in 5% NDS for 1 h at room temperature. Sections were then washed in TBS before being incubated in 0.05% ThioS in 50% ethanol for 8 min in the dark. Sections were then dunked in 80% ethanol 3 times for 10 s and then distilled water 3 times for 10 s before being counterstained with 1:1,000 DAPI, mounted using Immunomount, and imaged on an Olympus VS120-S6-W virtual slide microscope, at a magnification of 20×.

Statistical analyses

Statistical analyses were performed with the GraphPad Prism software unless otherwise stated. One-way ANOVA was used to analyze all between-group analyses, followed by Dunnett's multiple comparisons test between each group and the vehicle control. Simple linear regression analysis was used to assess the correlation between factors and the number of viral genome copies, with p values representing whether the slope was significantly nonzero. Viral genome copy number was log10 transformed, compared with the amount of APOE2 in the CSF, and assessed using a Boltzmann sigmoid curve. Statistics were performed where each mouse was a single data point, and an ROUT (robust regression and outlier removal) outlier test (Q = 1%) was performed on all datasets; no outliers were found unless otherwise stated. Samples were blinded for each analysis. Human data were assessed as a t test for microglial reactivity split by APOE4 status and as a simple linear regression where the number of APOE4 alleles was treated as an ordinal value, with APOE2/3 individuals considered to have −1 APOE4 alleles.

DATA AND CODE AVAILABILITY

The data that support the findings of this study are available from the corresponding author upon reasonable request.

SUPPLEMENTAL INFORMATION

Supplemental information can be found online at https://doi.org/10.1016/j.ymthe.2024.03.024.

ACKNOWLEDGMENTS

This study was supported by the NIH grants AG047644 (D.M.H.); NS090934 (D.M.H.); T32AG000222-27, P30AG062421, and U01NS111671 (B.L.D. and B.T.H.); RF1AG047644; the Children's Hospital of Philadelphia Research Institute; and the JPB Foundation.

AUTHOR CONTRIBUTIONS

R.J.J., B.L.D., and B.T.H. conceived the idea for the study. R.J.J., M.S.K., J.C.M., D.P.F., S.E.D., S.H., J.K., R.M., A.M., T.N., M.A.N., and L.T. were responsible for carrying out the experiments. R.J.J., M.S.K., L.T., P.T.R., E.C., Y.C., D.M.H., B.L.D., and B.T.H. were responsible for the methodology and resources. R.J.J. was responsible for writing the original draft, and R.J.J., M.S.K., P.T.R., E.C., D.M.H., W.H., B.L.D., and B.T.H. were responsible for reviewing, editing, and refining the final manuscript. R.J.J., B.T.H., D.M.H., W.H., and B.L.D. acquired the funding that supported this work.

DECLARATION OF INTERESTS

D.M.H. is on the scientific advisory board of C2N Diagnostics and has equity. D.M.H. is on the scientific advisory board of Denali Therapeutics, Genentech, and Cajal Therapeutics and consults for Asteroid. B.L.D. serves an advisory role with equity in Latus Biosciences, Patch Bio, Voyager Therapeutics, Carbon Biosciences, Spirovant Biosciences, Resilience, Panorama Medicines, Saliogen, and Homology Medicines. She has sponsored research from Novartis, Roche, Latus, Homology Medicines, Saliogen, and Spirovant. B.T.H. is on the scientific advisory board of Latus Bio and has an equity interest. B.T.H. has a family member who works at Novartis, and owns stock in Novartis; he serves on the scientific advisory board of Dewpoint and owns stock. He serves on a scientific advisory board of or is a consultant for AbbVie, Aprinoia Therapeutics, Arvinas, Avrobio, Axial, Biogen, BMS, Cure Alzheimer's Fund, Cell Signaling, Dewpoint, Eisai, Genentech, Ionis, Latus, Novartis, Sangamo, Sanofi, Seer, Takeda, the US Department of Justice, Vigil, and Voyager. M.S.K., L.T., Y.C., and P.T.R. are founders of and shareholders in Latus Biosciences.

REFERENCES

1. Corder, E.H., Saunders, A.M., Strittmatter, W.J., Schmechel, D.E., Gaskell, P.C., Small, G.W., Roses, A.D., Haines, J.L., and Pericak-Vance, M.A. (1993). Gene dose of apolipoprotein E type 4 allele and the risk of Alzheimer's disease in late onset families. Science *261*, 921–923. https://doi.org/10.1126/science.8346443.

2. Corder, E.H., Saunders, A.M., Risch, N.J., Strittmatter, W.J., Schmechel, D.E., Gaskell, P.C., Rimmler, J.B., Locke, P.A., Conneally, P.M., and Schmader, K.E. (1994). Protective effect of apolipoprotein E type 2 allele for late onset Alzheimer disease. Nat. Genet. *7*, 180–184. https://doi.org/10.1038/ng0694-180.

3. AlzGene (2017). AlzGene. http://www.alzgene.org/meta.asp?geneID=83.

4. Rebeck, G.W., Reiter, J.S., Strickland, D.K., Hyman, B.T., William Rebeck, G., Reiter, J.S., Strickland, D.K., and Hyman, B.T. (1993). Apolipoprotein E in sporadic Alzheimer's disease: Allelic variation and receptor interactions. Neuron *11*, 575–580. https://doi.org/10.1016/0896-6273(93)90070-8.

5. Reiman, E.M., Arboleda-Velasquez, J.F., Quiroz, Y.T., Huentelman, M.J., Beach, T.G., Caselli, R.J., Chen, Y., Su, Y., Myers, A.J., Hardy, J., et al. (2020). Exceptionally low likelihood of Alzheimer's dementia in APOE2 homozygotes from a 5,000-person neuropathological study. Nat. Commun. *11*, 667. https://doi.org/10.1038/s41467-019-14279-8.

6. West, H.L., Rebeck, G.W., and Hyman, B.T. (1994). Frequency of the apolipoprotein E epsilon 2 allele is diminished in sporadic Alzheimer disease. Neurosci. Lett. *175*, 46–48. https://doi.org/10.1016/0304-3940(94)91074-X.

7. Serrano-Pozo, A., Das, S., and Hyman, B.T. (2021). APOE and Alzheimer's disease: advances in genetics, pathophysiology, and therapeutic approaches. Lancet Neurol. *20*, 68–80. https://doi.org/10.1016/S1474-4422(20)30412-9.

8. Serrano-Pozo, A., Qian, J., Monsell, S.E., Betensky, R.A., and Hyman, B.T. (2015). APOEε2 is associated with milder clinical and pathological Alzheimer's disease. Ann. Neurol. *77*, 917–929. https://doi.org/10.1002/ana.24369.

9. Castellano, J.M., Kim, J., Stewart, F.R., Jiang, H., DeMattos, R.B., Patterson, B.W., Fagan, A.M., Morris, J.C., Mawuenyega, K.G., Cruchaga, C., et al. (2011). Human apoE isoforms differentially regulate brain amyloid-beta peptide clearance. Sci. Transl. Med. *3*, 89ra57. https://doi.org/10.1126/scitranslmed.3002156.

10. Deane, R., Sagare, A., Hamm, K., Parisi, M., Lane, S., Finn, M.B., Holtzman, D.M., and Zlokovic, B.V. (2008). apoE isoform – specific disruption of amyloid β peptide clearance from mouse brain. J. Clin. Invest. *118*, 4002–4013. https://doi.org/10.1172/JCI36663DS1.

11. Garai, K., Verghese, P.B., Baban, B., Holtzman, D.M., and Frieden, C. (2014). The Binding of Apolipoprotein E to Oligomers and Fibrils of Amyloid-β Alters the Kinetics of Amyloid Aggregation. Biochemistry *53*, 6323–6331. https://doi.org/10.1021/bi5008172.

12. Hashimoto, T., Serrano-Pozo, A., Hori, Y., Adams, K.W., Takeda, S., Banerji, A.O., Mitani, A., Joyner, D., Thyssen, D.H., Bacskai, B.J., et al. (2012). Apolipoprotein E, Especially Apolipoprotein E4, Increases the Oligomerization of Amyloid Peptide. J. Neurosci. *32*, 15181–15192. https://doi.org/10.1523/JNEUROSCI.1542-12.2012.

13. Fagan, A.M., Watson, M., Parsadanian, M., Bales, K.R., Paul, S.M., and Holtzman, D.M. (2002). Human and murine ApoE markedly alters A beta metabolism before and after plaque formation in a mouse model of Alzheimer's disease. Neurobiol. Dis. *9*, 305–318. https://doi.org/10.1006/nbdi.2002.0483.

14. Shi, Y., Yamada, K., Liddelow, S.A., Smith, S.T., Zhao, L., Luo, W., Tsai, R.M., Spina, S., Grinberg, L.T., Rojas, J.C., et al. (2017). ApoE4 markedly exacerbates tau-mediated neurodegeneration in a mouse model of tauopathy. Nature *549*, 523–527. https://doi.org/10.1038/nature24016.

15. Klein, R.C., Mace, B.E., Moore, S.D., and Sullivan, P.M. (2010). Progressive loss of synaptic integrity in human apolipoprotein E4 targeted replacement mice and attenuation by apolipoprotein E2. Neuroscience *171*, 1265–1272. https://doi.org/10.1016/j.neuroscience.2010.10.027.

16. Koffie, R.M., Hashimoto, T., Tai, H.-C., Kay, K.R., Serrano-Pozo, A., Joyner, D., Hou, S., Kopeikina, K.J., Frosch, M.P., Lee, V.M., et al. (2012). Apolipoprotein E4 effects in Alzheimer's disease are mediated by synaptotoxic oligomeric amyloid-β. Brain *135*, 2155–2168. https://doi.org/10.1093/brain/aws127.

17. Serrano-Pozo, A., Li, Z., Noori, A., Nguyen, H.N., Mezlini, A., Li, L., Hudry, E., Jackson, R.J., Hyman, B.T., and Das, S. (2021). Effect of APOE alleles on the glial transcriptome in normal aging and Alzheimer's disease. Nat. Aging *1*, 919–931. https://doi.org/10.1038/s43587-021-00123-6.

18. Chernick, D., Ortiz-Valle, S., Jeong, A., Qu, W., and Li, L. (2019). Peripheral versus central nervous system APOE in Alzheimer's disease: Interplay across the blood-brain barrier. Neurosci. Lett. *708*, 134306. https://doi.org/10.1016/j.neulet.2019.134306.

19. Hudry, E., Dashkoff, J., Roe, A.D., Takeda, S., Koffie, R.M., Hashimoto, T., Scheel, M., Spires-Jones, T., Arbel-Ornath, M., Betensky, R., et al. (2013). Gene transfer of human Apoe isoforms results in differential modulation of amyloid deposition and neurotoxicity in mouse brain. Sci. Transl. Med. *5*, 212ra161. https://doi.org/10.1126/scitranslmed.3007000.

20. Rosenberg, J.B., Kaplitt, M.G., De, B.P., Chen, A., Flagiello, T., Salami, C., Pey, E., Zhao, L., Ricart Arbona, R.J., Monette, S., et al. (2018). AAVrh.10-Mediated APOE2 Central Nervous System Gene Therapy for APOE4-Associated Alzheimer's Disease. Hum. Gene Ther. Clin. Dev. *29*, 24–47. https://doi.org/10.1089/humc.2017.231.

21. Zhao, L., Gottesdiener, A.J., Parmar, M., Li, M., Kaminsky, S.M., Chiuchiolo, M.J., Sondhi, D., Sullivan, P.M., Holtzman, D.M., Crystal, R.G., and Paul, S.M. (2016). Intracerebral adeno-associated virus gene delivery of apolipoprotein E2 markedly reduces brain amyloid pathology in Alzheimer's disease mouse models. Neurobiol. Aging *44*, 159–172. https://doi.org/10.1016/J.NEUROBIOLAGING.2016.04.020.

22. Dickson, P., McEntee, M., Vogler, C., Le, S., Levy, B., Peinovich, M., Hanson, S., Passage, M., and Kakkis, E. (2007). Intrathecal enzyme replacement therapy: successful treatment of brain disease via the cerebrospinal fluid. Mol. Genet. Metab. *91*, 61–68. https://doi.org/10.1016/j.ymgme.2006.12.012.

23. Ichimura, T., Fraser, P.A., and Cserr, H.F. (1991). Distribution of extracellular tracers in perivascular spaces of the rat brain. Brain Res. *545*, 103–113. https://doi.org/10.1016/0006-8993(91)91275-6.

24. Katz, M.L., Tecedor, L., Chen, Y., Williamson, B.G., Lysenko, E., Wininger, F.A., Young, W.M., Johnson, G.C., Whiting, R.E.H., Coates, J.R., and Davidson, B.L. (2015). AAV gene transfer delays disease onset in a TPP1-deficient canine model of the late infantile form of Batten disease. Sci. Transl. Med. *7*, 313ra180. https://doi.org/10.1126/scitranslmed.aac6191.

25. Carrell, E.M., Chen, Y.H., Ranum, P.T., Coffin, S.L., Singh, L.N., Tecedor, L., Keiser, M.S., Hudry, E., Hyman, B.T., and Davidson, B.L. (2023). VWA3A-derived ependyma promoter drives increased therapeutic protein secretion into the CSF. Mol. Ther. Nucleic Acids *33*, 296–304. https://doi.org/10.1016/j.omtn.2023.07.016.

26. Huynh, T.P.V., Wang, C., Tran, A.C., Tabor, G.T., Mahan, T.E., Francis, C.M., Finn, M.B., Spellman, R., Manis, M., Tanzi, R.E., et al. (2019). Lack of hepatic apoE does not influence early Aβ deposition: Observations from a new APOE knock-in model. Mol. Neurodegener. *14*, 37. https://doi.org/10.1186/s13024-019-0337-1.

27. Radde, R., Bolmont, T., Kaeser, S.A., Coomaraswamy, J., Lindau, D., Stoltze, L., Calhoun, M.E., Jäggi, F., Wolburg, H., Gengler, S., et al. (2006). Aβ42-driven cerebral amyloidosis in transgenic mice reveals early and robust pathology. EMBO Rep. *7*, 940–946. https://doi.org/10.1038/sj.embor.7400784.

28. Chen, W.-T., Lu, A., Craessaerts, K., Pavie, B., Sala Frigerio, C., Corthout, N., Qian, X., Laláková, J., Kühnemund, M., Voytyuk, I., et al. (2020). Spatial Transcriptomics and In Situ Sequencing to Study Alzheimer's Disease. Cell *182*, 976–991.e19. https://doi.org/10.1016/j.cell.2020.06.038.

29. Krasemann, S., Madore, C., Cialic, R., Baufeld, C., Calcagno, N., El Fatimy, R., Beckers, L., O'Loughlin, E., Xu, Y., Fanek, Z., et al. (2017). The TREM2-APOE Pathway Drives the Transcriptional Phenotype of Dysfunctional Microglia in Neurodegenerative Diseases. Immunity *47*, 566–581.e9. https://doi.org/10.1016/J.IMMUNI.2017.08.008.

30. Yamamoto, T., Choi, H.W., and Ryan, R.O. (2008). Apolipoprotein E isoform-specific binding to the low-density lipoprotein receptor. Anal. Biochem. *372*, 222–226. https://doi.org/10.1016/j.ab.2007.09.005.

31. Liu, G., Martins, I., Wemmie, J.A., Chiorini, J.A., and Davidson, B.L. (2005). Functional Correction of CNS Phenotypes in a Lysosomal Storage Disease Model Using Adeno-Associated Virus Type 4 Vectors. J. Neurosci. *25*, 9321–9327. https://doi.org/10.1523/JNEUROSCI.2936-05.2005.

32. Jiménez, A.J., Domínguez-Pinos, M.D., Guerra, M.M., Fernández-Llebrez, P., and Pérez-Fígares, J.M. (2014). Structure and function of the ependymal barrier and diseases associated with ependyma disruption. Tissue Barriers *2*, e28426. https://doi.org/10.4161/tisb.28426.

33. Efthymiou, A.G., and Goate, A.M. (2017). Late onset Alzheimer's disease genetics implicates microglial pathways in disease risk. Mol. Neurodegener. *12*, 43. https://doi.org/10.1186/s13024-017-0184-x.

34. Hong, S., Beja-Glasser, V.F., Nfonoyim, B.M., Frouin, A., Li, S., Ramakrishnan, S., Merry, K.M., Shi, Q., Rosenthal, A., Barres, B.A., et al. (2016). Complement and microglia mediate early synapse loss in Alzheimer mouse models. Science *352*, 712–716. https://doi.org/10.1126/science.aad8373.

35. Leng, F., and Edison, P. (2021). Neuroinflammation and microglial activation in Alzheimer disease: where do we go from here? Nat. Rev. Neurol. *17*, 157–172. https://doi.org/10.1038/s41582-020-00435-y.

36. Wang, Y., Ulland, T.K., Ulrich, J.D., Song, W., Tzaferis, J.A., Hole, J.T., Yuan, P., Mahan, T.E., Shi, Y., Gilfillan, S., et al. (2016). TREM2-mediated early microglial response limits diffusion and toxicity of amyloid plaques. J. Exp. Med. *213*, 667–675. https://doi.org/10.1084/jem.20151948.

37. Meilandt, W.J., Ngu, H., Gogineni, A., Lalehzadeh, G., Lee, S.-H., Srinivasan, K., Imperio, J., Wu, T., Weber, M., Kruse, A.J., et al. (2020). Trem2 Deletion Reduces Late-Stage Amyloid Plaque Accumulation, Elevates the Aβ42:Aβ40 Ratio, and Exacerbates Axonal Dystrophy and Dendritic Spine Loss in the PS2APP Alzheimer's Mouse Model. J. Neurosci. *40*, 1956–1974. https://doi.org/10.1523/JNEUROSCI.1871-19.2019.

38. Jackson, R.J., Rose, J., Tulloch, J., Henstridge, C., Smith, C., and Spires-Jones, T.L. (2019). Clusterin accumulates in synapses in Alzheimer's disease and is increased in apolipoprotein E4 carriers. Brain Commun. *1*, fcz003. https://doi.org/10.1093/braincomms/fcz003.

39. Koffie, R.M., Hyman, B.T., Spires-Jones, T.L., Alzheimer, A., Goedert, M., Spillantini, M., Hebert, L., Scherr, P., Bienias, J., Bennett, D., et al. (2011). Alzheimer's disease: synapses gone cold. Mol. Neurodegener. *6*, 63. https://doi.org/10.1186/1750-1326-6-63.

40. Budd Haeberlein, S., Aisen, P.S., Barkhof, F., Chalkias, S., Chen, T., Cohen, S., Dent, G., Hansson, O., Harrison, K., von Hehn, C., et al. (2022). Two Randomized Phase 3 Studies of Aducanumab in Early Alzheimer's Disease. J. Prev. Alzheimers Dis. *9*, 197–210. https://doi.org/10.14283/jpad.2022.30.

41. van Dyck, C.H., Swanson, C.J., Aisen, P., Bateman, R.J., Chen, C., Gee, M., Kanekiyo, M., Li, D., Reyderman, L., Cohen, S., et al. (2023). Lecanemab in Early Alzheimer's Disease. N. Engl. J. Med. *388*, 9–21. https://doi.org/10.1056/NEJMoa2212948.

42. Li, J., Cai, Z., Bomgarden, R.D., Pike, I., Kuhn, K., Rogers, J.C., Roberts, T.M., Gygi, S.P., and Paulo, J.A. (2021). TMTpro-18plex: The Expanded and Complete Set of TMTpro Reagents for Sample Multiplexing. J. Proteome Res. *20*, 2964–2972. https://doi.org/10.1021/acs.jproteome.1c00168.

43. Edwards, A., and Haas, W. (2016). Multiplexed Quantitative Proteomics for High-Throughput Comprehensive Proteome Comparisons of Human Cell Lines. Methods Mol. Biol. *1394*, 1–13. https://doi.org/10.1007/978-1-4939-3341-9_1.

44. Hughes, C.S., Moggridge, S., Müller, T., Sorensen, P.H., Morin, G.B., and Krijgsveld, J. (2019). Single-pot, solid-phase-enhanced sample preparation for proteomics experiments. Nat. Protoc. *14*, 68–85. https://doi.org/10.1038/s41596-018-0082-x.

45. Hashimoto, T., Fujii, D., Naka, Y., Kashiwagi-Hakozaki, M., Matsuo, Y., Matsuura, Y., Wakabayashi, T., and Iwatsubo, T. (2020). Collagenous Alzheimer amyloid plaque component impacts on the compaction of amyloid-β plaques. Acta Neuropathol. Commun. *8*, 212. https://doi.org/10.1186/s40478-020-01075-5.

46. Bankhead, P., Loughrey, M.B., Fernández, J.A., Dombrowski, Y., McArt, D.G., Dunne, P.D., McQuaid, S., Gray, R.T., Murray, L.J., Coleman, H.G., et al. (2017). QuPath: Open source software for digital pathology image analysis. Sci. Rep. *7*, 16878. https://doi.org/10.1038/s41598-017-17204-5.